Hindawi
Journal of Advanced Transportation
Volume 2019, Article ID 6326794, 12 pages
https://doi.org/10.1155/2019/6326794

Research Article

Numerical Simulation of the Static and Dynamic Aerodynamics of a UAV under Wake Flows

Bai-gang Mi[1] **and Hao Zhan**[2]

[1]*School of Aerospace Engineering, Tsinghua University, Beijing 100084, China*
[2]*School of Aeronautics, Northwestern Polytechnical University, Xi'an, Shaanxi 710072, China*

Correspondence should be addressed to Bai-gang Mi; mibaigang@163.com

Received 23 October 2018; Revised 7 January 2019; Accepted 13 March 2019; Published 1 April 2019

Academic Editor: Andrea Monteriù

Frequent flight conflicts will be observed as the number of aircrafts increases, and such conflicts will cause unprecedented challenges in flight safety; thus, the flight characteristics of small aircrafts under the wake flow of a large airliner should be thoroughly analyzed. Combined with the sliding mesh technique, a computational fluid dynamics (CFD) method is proposed in this paper to simulate three wake flow patterns, i.e., wingtip vortex, jet flow, and propeller slipstream, and then, the static and dynamic derivatives that represent the stability of the fly wing under the wake flow are identified by using the least squares method. The results demonstrate that both the steady and unsteady aerodynamics of the fly wing are affected by wake flows: wingtip vortices increase the lift-to-drag ratio and considerably change the dynamic damping; jet flow reduces both the static and dynamic damping; and propeller slipstream leads to slow variations in the dynamic damping and decreases in the lift-to-drag ratio.

1. Introduction

Improvements in aeronautical techniques and increased demand have led to an increasing number of flight vehicles in various fields. According to forecasts by Boeing, over 50000 large jets will be required in the coming decades. Thus, air traffic systems will be tasked with addressing this increased congestion, and frequent flight conflicts will place unprecedented pressure on control systems and threaten flight safety. One of the negative phenomena related to flight congestion is the impact of the wake of the front aircraft on the rear aircraft, and this phenomenon has caused several air crashes in the history of aircraft. Moreover, the wake effect [1] should also be considered for military aircraft, such as during aerial refueling, because accurate control of the refueling aircraft in the wake flow of a large aerial tanker is a challenging task. Thus, to ensure flight safety and improve the task completion efficiency, the effect of a wake on the aerodynamics of small aircraft should be analyzed in detail.

The wake flows of large aircraft can be divided into the following aspects: wingtip vortex [2], jet flow [3], propeller slipstream [4], and wing-body turbulence. Wingtip vortices are circular patterns of rotating air that trail behind a wing as it generates lift, and they eventually roll up into large vortices near the wingtip. The jet flow generated by a jet engine could present high temperatures and speeds and thus could have a considerable impact on the rear airplane. The propeller slipstream is highly complex because of the self-induced velocities produced by the propeller vortex system; thus, the slipstream tends to deform and roll up to produce a so-called slipstream tube, which presents strong gradients in various directions. The turbulence of the wing-body is mainly caused by the spanwise flow on the surface of the wing and the body of the aircraft. Among all the wake flow patterns, the aerodynamic impacts of the first three types are the most important and will be analyzed in detail in this paper.

In recent decades, many studies have been conducted to simulate wingtip vortices. Dacles-Mariani [5] used the one-equation Baldwin-Barth turbulence model to calculate the behavior of wingtip vortex flow. The results indicated that the model could describe the basic aerodynamic characteristics but could not accurately capture the detailed structures of the vortex. Li [6] adopted a Large Eddy Simulation with a filtered-structure-function subgrid model to simulate the

wingtip vortex of a rectangular half-wing with a NACA 0012 airfoil section and a rounded wingtip. The calculations demonstrated that this model was much more accurate than traditional Reynolds Average Navier-Stokes (RANS) methods and could better reveal the detailed characteristics of vortices. Matthew [7] investigated the accuracy of current state-of-the-art turbulence models and a compressible RANS solver model at simulating the formation of a wingtip vortex in the near field, and he found that these models predicted the mean flow accurately; however, none of them could accurately capture the magnitudes of the turbulence quantities or the lag of the Reynolds stress components underlying the corresponding strain-rate components. Moreover, many scholars have also studied the influence of wingtip vortices in formation flight. Inasawa [8] investigated the static aerodynamic interactions of wingtip vortices in close-formation of two wings that consist of the NACA 23012 airfoil section. The results showed that the tip vortices of the leading and trail wings interacted closely with each other to form a pair of counterrotating vortices for smaller overlap conditions of less than 5% with zero vertical offset. Kasper [9] had used both experimental and computational approaches to analyze in detail the upwash generated from the wingtip vortices of the formation flight for UAVs. The results revealed that formation flying can benefit flight performance in many ways and that altering the formation can lead to different benefits depending on the configuration.

A series of studies have also been conducted on the jet flow. Rudnik [10] evaluated the influence of increasing the bypass ratio and varying the position on the ALVAST narrow body wing/fuselage model using a numerical method. The investigations showed that the lift loss is proportional to the engine size and alleviated by the upstream movement of the engine position. Ritter [11] used the RANS-CFD method to investigate the strong impacts of Ultra-High-Bypass-Ratio (UHBR)-Engines on the aerodynamics of high-lift wings. The results of the study mainly focused on the effects of engine position on the achievable maximum lift coefficient and lift-to-drag ratio to identify an optimal engine position related to high-lift performance. Melber-Wilkending [12] considered the numerical solutions of the aerodynamics of two different configurations with an open and a closed thrust-gate by using RANS equations. The results indicated that, with an increased angle of attack, a flattening of the jet hull occurred at the upper side, and an increase in sidewise spreading was detected. The closed thrust-gate caused a more distinctive effect, with the inboard flap being partially passed by the engine jet.

Studies on propeller slipstream have been conducted for a long time. Schroijen [13] developed a tool to estimate the propeller slipstream effects on directional control in the critical case of a failed engine. Based on vortex theory, this simple model can quickly evaluate the sign and magnitude of the slipstream effects on the engine-out yawing moment. Moens [14] presented two numerical studies of the propeller/wing interactions for transport aircraft. The first one used the Euler conditions to compute a three-element high-lift section in take-off configuration and analyzed the details of the complex slipstream flow interactions on the flap system, and the second case evaluated the global performance of a four-propeller generic transport aircraft with a N-S solver and correctly predicted the blowing effect. Similar work was performed by Lenfers [15] and Xu [16], who used a computational method to study the propeller and high-lift wing interaction with different RANS and grid forms. Khan [17] presented a slipstream model that considered both the acceleration and diffusion phenomena via simple analytical and semiempirical equations to accurately predict the induced velocity at up to 8-10 propeller diameters downstream of the propeller plane.

Although recent research on wingtip vortices, jet flow and propeller slipstream mainly focused on the impacts of these phenomena on the airplane itself, few works have investigated the wake flow effects on the static and dynamic aerodynamics in aircraft formation.

The present study proposes a method that combines high-fidelity computational fluid dynamics (CFD) and a sliding mesh technique to assess the static and dynamic aerodynamics of the fly wing configuration [18, 19] under the effects of wingtip vortices, jet flow, and propeller slipstream, and the corresponding derivatives are also identified to evaluate the stability of the aircraft. The methods and conclusions obtained in this paper can provide detailed explanations of the aerodynamic characteristics of aircraft in wake flows and additional technical support for flight control system design.

2. Numerical Method

2.1. Governing Equation. The 3D Reynolds average N-S equation used to describe the flow field is expressed as

$$\frac{\partial}{\partial t}\iiint_V \mathbf{W}dV + \iint_{\partial \mathbf{V}} \mathbf{F} \bullet \mathbf{n}ds = \frac{1}{\mathrm{Re}} \iint_{\partial V} \mathbf{F}_\mathbf{v} \bullet \mathbf{n}ds \quad (1)$$

where V indicates the control volume, $\mathbf{W}$ denotes the vector of conserved variables, $\mathbf{F}$ is the inviscid component of the flux vectors, $\mathbf{F}_\mathbf{v}$ represents the viscous flux vector, and Re is the Reynolds number.

The two-equation turbulence model called the shear-stress transport (SST) $k - \omega$ model is used in this paper to calculate the cases. Developed by Menter [20], this model takes the transport of the turbulent shear stress into the Wilcox $k - \omega$ model to give highly accurate predictions of the onset and the amount of flow separation under adverse pressure gradients. A sliding mesh technique is adopted to simulate the dynamic motion in all the unsteady cases. The sliding mesh is a special case of a general dynamic mesh motion in which all the cells move rigidly in a specific dynamic zone. This technique employs two or more cell zones, and each cell zone is bounded by at least one interface zone, where it meets the opposing cell zone. The interface zones of adjacent cell zones are associated with one another to form a mesh interface. During the unsteady calculation, the cell zones slide relative to one another along the interface in discrete steps.

2.2. Static and Dynamic Derivative Identification. Static derivatives are generally obtained by traditional methods via interpolations of steady aerodynamic forces and moments,

whereas dynamic derivatives are calculated with the single-point or integration method by imposing a forced sinusoidal motion around the aircraft center of gravity. However, the artificial separation of static and dynamic derivative identifications may lead to substantial errors, especially in cases with nonlinear characteristics.

In this paper, we use a new method to simultaneously compute static and dynamic derivatives [21, 22] that is based on the aerodynamics model and incorporates unsteady aerodynamic forces and moments of forced sinusoidal motion.

The unsteady aerodynamic model of forced motion at small angles of attack (AoAs) can be expressed as

$$C_i = C_{i0} + C_{i\alpha}\Delta\alpha + C_{i\dot{\alpha}}\hat{\dot{\alpha}} + o(\alpha) \tag{2}$$

where $i = L, D, M$ (indicating the lift, drag, and moment, respectively); C_i represents the unsteady force or moment coefficient; $C_{i\alpha}$ denotes the static derivatives and is used to evaluate the trend that the aircraft moves back to original balanced state with restoring moments; $C_{i\dot{\alpha}}$ is the dynamic derivative focused on the time response process with disturbance; and $\hat{\dot{\alpha}} = \dot{\alpha}c/2V$ denotes the nondimensional rate of the AoA.

When discarding the high-order terms $o(\alpha)$, the frequently used aerodynamic derivatives model is given as

$$C_i = C_{i0} + C_{i\alpha}\Delta\alpha + C_{i\dot{\alpha}}\hat{\dot{\alpha}} \tag{3}$$

Because the rate of the AoA $\dot{\alpha}$ and angular velocity q have the same form when the freestream remains unchanged, they are difficult to separate and are often denoted as

$$C_{i\dot{\alpha}} = C_{i\dot{\alpha}} + C_{iq} \tag{4}$$

This term is referred to as the combined dynamic derivatives.

The model is fit to most cases at a small AoA with linear or weak nonlinear aerodynamic characteristics. Moreover, we use the least squares method to identify the static and dynamic derivatives.

2.3. Method Validation with SACCON Configuration. A generic UCAV called SACCON (Stability and Control CONfiguration), which is used by an Applied Vehicle Technology Task Group (AVT-161) established by the NATO Research and Technology Organization (RTO), is adopted to verify the method, and the relevant static and dynamic aerodynamics are measured in the Low Speed Wind Tunnel Braunschweig (DNW-NWB) [23].

The model contains a lambda wing with a leading-edge sweep angle of 53°, as shown in Figure 1. The root chord is approximately 1 m, the wing span is 1.53 m, the mean aerodynamic chord is 0.479 m, and the reference wing area is 0.77 m^2. The moment reference point (MRP) is located 0.6 m from the head of the wing, and the point of rotation (POR) for dynamic testing is 0.255414 m behind the MRP.

We firstly evaluate the static cases of the single fly wing to understand its aerodynamic performance. Comparisons of lift and pitching moment coefficient are, respectively, shown

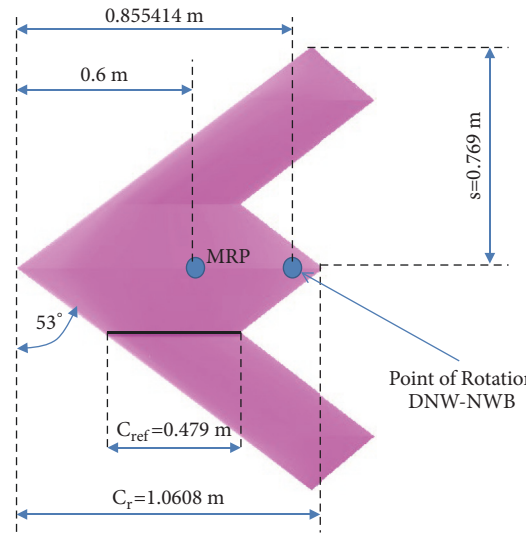

Figure 1: Geometric parameters of the SACCON UCAV configuration.

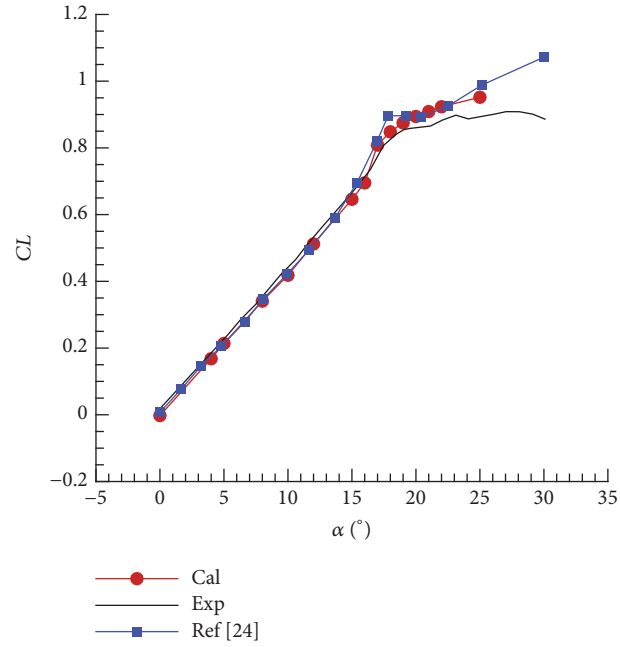

Figure 2: Lift coefficients.

in Figures 2 and 3. The lift coefficients have good agreement with the wind tunnel data or the calculating data in [24] below 17 degrees, while both the lift coefficients calculation and reference data diverge when ranging up to larger angle of attack. Therefore, none of the simulations well match the test data. The changing process of pitching moment coefficients are more complicated with the increment of the angle of attack. First of all, both the calculation and reference data have bad agreement with the experiment results when the angle of attack is below nearly 15 degrees, including the magnitude and slope of profiles. The possible reason may be that the sting and wind tunnel wall effects are not considered

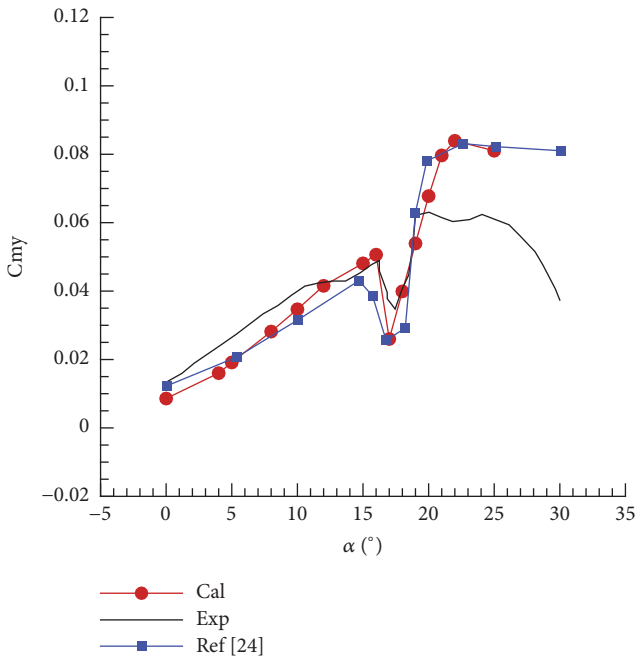

Figure 3: Pitching moment coefficients.

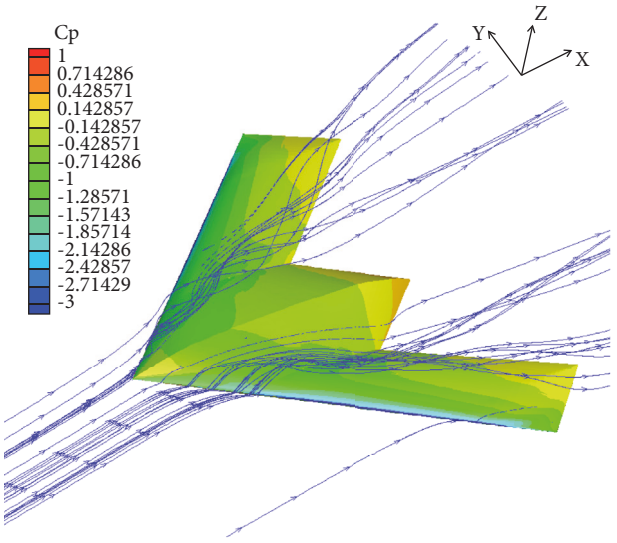

Figure 4: Leading-edge vortex at AoA=15°.

in the simulation. The predictions become better when the angle of attack increases further. All the methods capture the sharp reduction in nose-up pitching moment, with a sharp increase afterwards in positive moment between 17 and 20 degrees. This indicates that all the methods can well describe the basic vortex variations during the static process, shown in Figure 4.

Then we calculate the dynamic motion with sliding mesh technique to identify the stability derivatives. The validation case of a single fly wing without a sting is considered using the same conditions as those of the wind tunnel test (Table 1). Based on the method in this paper, the static and dynamic

Table 1: Simulation conditions.

Parameters	Values
Mach number Ma	0.146
Reynolds number based on reference chord c	1.13×10^6
Initial AoA α_0	0°
Reduced frequency k	0.090289397
Additional angle of attack $\triangle\alpha$	$1^\circ \sin(6\pi t)$

Table 2: Calculation results of static and dynamic derivatives.

Stability derivatives	Calculation	Wind tunnel test	Error
Static derivative $C_{z\alpha}$	1.49487	1.3752	8.7%
Dynamic derivative $C_{m\dot{\alpha}} + C_{mq}$	-0.76599	-0.82	6.59%

derivatives are calculated and shown in Table 2, and they are consistent with the wind tunnel test data [24].

3. Computational Models and Grids

Three wake flow types are considered here: wingtip vortices, jet flow, and propeller slipstream. The following computational models (Figure 5) are used: a combined airliner and fly wing model is used to simulate the effect of wingtip vortices; the power-on wing-body and fly wing models are used to calculate the jet flow; and a wing-body model with a propeller is applied to evaluate the interference on the fly wing. Except for the spanwise and chordwise locations, the fly wings have the same flight attitude with the large aircrafts ahead in three models. Moreover, the sizes of the fly wings have been adjusted to match the large aircrafts. Compared to the standard SACCON configuration, the spans for wingtip vortex and jet flow simulations are extended to $7m$, while the value is changed to $4.5m$ due to the relatively small size of the propeller aircraft. It is noted that the three models in this paper are just selected to analyze the static and dynamic aerodynamics of a small UAV under the wake flows of large aircrafts, they may be something different from actual cases, but it is similar in methods and results.

The commercial software ANSYS ICEM CFD (Pittsburgh, Pennsylvania, USA) is used to generate the computational mesh. Based on the sliding mesh technique, the flow field can be divided into two zones: the inner dynamic zone with the fly wing and the outer static zone with the civil aircraft. An interface is set up to connect the two zones. The unstructured computational grids are shown in Figure 6. The mesh cells are clustered around the leading edges. As the reason that the wake flows are difficult to capture due to numerical dissipation of CFD methods, we set a mesh refined zone to improve the accuracy of solutions, seen in Figure 5, where adequate volume meshes have been enhanced to describe the true flow fields.

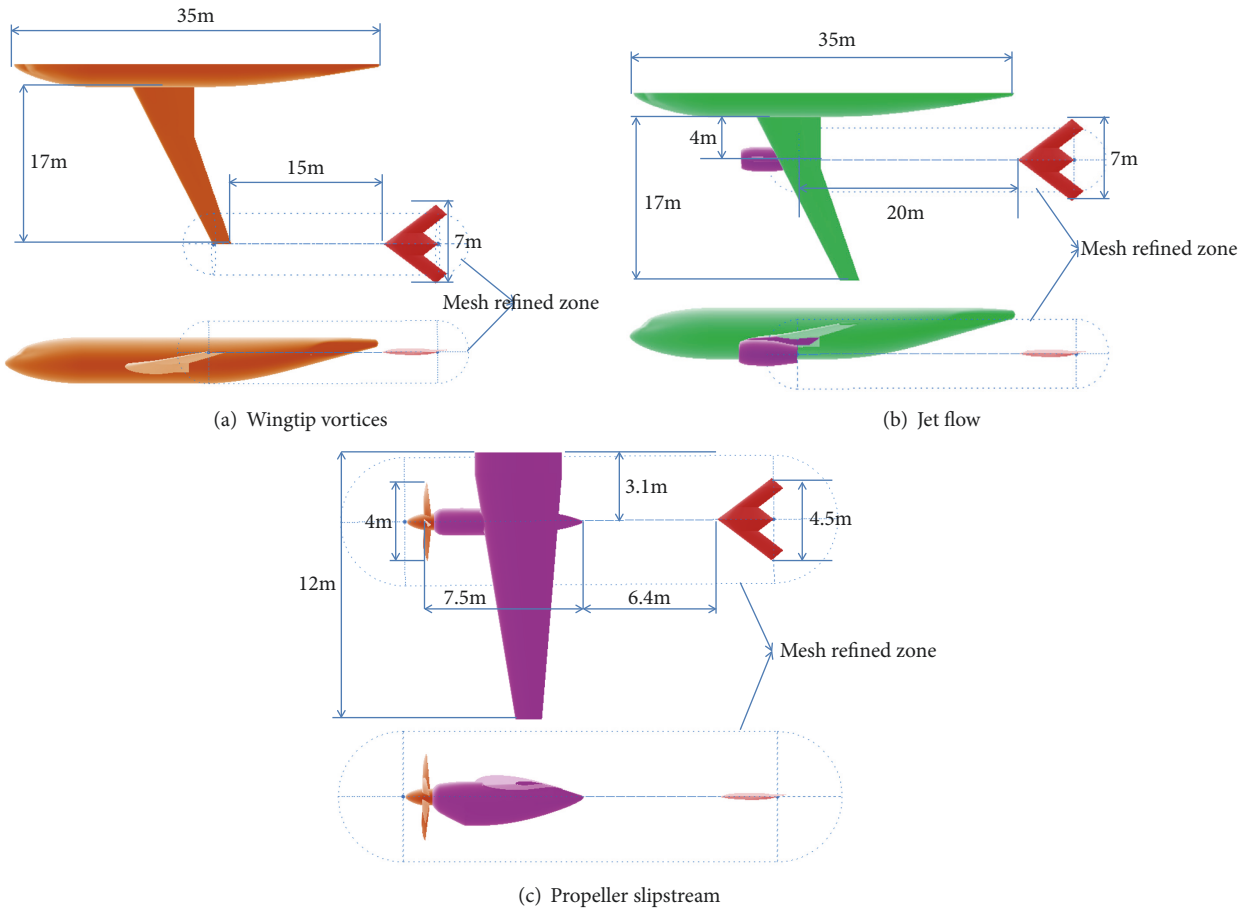

(a) Wingtip vortices

(b) Jet flow

(c) Propeller slipstream

FIGURE 5: Computational models.

4. Calculation Results

Using the method discussed earlier in this paper, we initially perform steady case simulations, and these results can be used to further calculate unsteady motions. The static and dynamic derivatives can be then identified via the unsteady aerodynamic forces and moments.

4.1. Effect of Wingtip Vortices. For a large airliner, the wingtip vortices are apparently strong and cause a wide range of effects. To improve the accuracy and reduce the numerical dissipation, the computational grids around and behind the wingtip were refined. We choose the representative cruise mode with a Mach number of 0.7 and altitude of 11 *km* as the simulation conditions, and the attitude of the airliner remains unchanged while the fly wing oscillates around its center of gravity with three different AoAs: 0, 5, and 10 degrees.

Figure 7 shows the vorticity values of the airliner's wingtip vortex, which indicates that the wingtip can extend a long distance to affect the aerodynamic characteristics of the flight vehicles under this flow. Figures 8 and 9 display a comparison of the steady aerodynamics between the wingtip vortices and the single fly wing cases. The results show that both the lift and drag coefficients have been enhanced under increases of the AoA, with slightly greater increases in the lift, which indicates that the lift-to-drag ratio can be improved via increases in the AoA. These results explain why the formation of fly wings is always used during the actual flight. Moreover, the pitching and yawing moment coefficients do not show significant changes compared with the single fly wing cases. However, because of the shearing velocity of the wingtip vortices, unbalanced forces develop on two sides of the fly wing and cause positive rolling moments to appear.

The static and dynamic derivatives obtained by using the least squares method are shown in Figures 10 and 11. Because the steady pitching moments remain unchanged at small AoAs, the static derivatives are nearly the same as those of single fly wing cases, indicating that the static stabilities are weakly affected by the wingtip vortices of the airliner. However, the dynamic derivatives are heavily affected by this wake flow, and although the values are negative and the fly wing still exhibits dynamic damping, the vortices cause greater damping as well as local dynamic stabilities at 0° and 5° AoAs compared with normal cases. When the AoA increases to 10°, the effect is weakened via the small flow separation on surface of the fly wing.

4.2. Effect of Jet Flow. To simulate the inner and outer flows in a real flight, the effect of engine power must be considered. A jet flow with high temperatures and speeds affects not

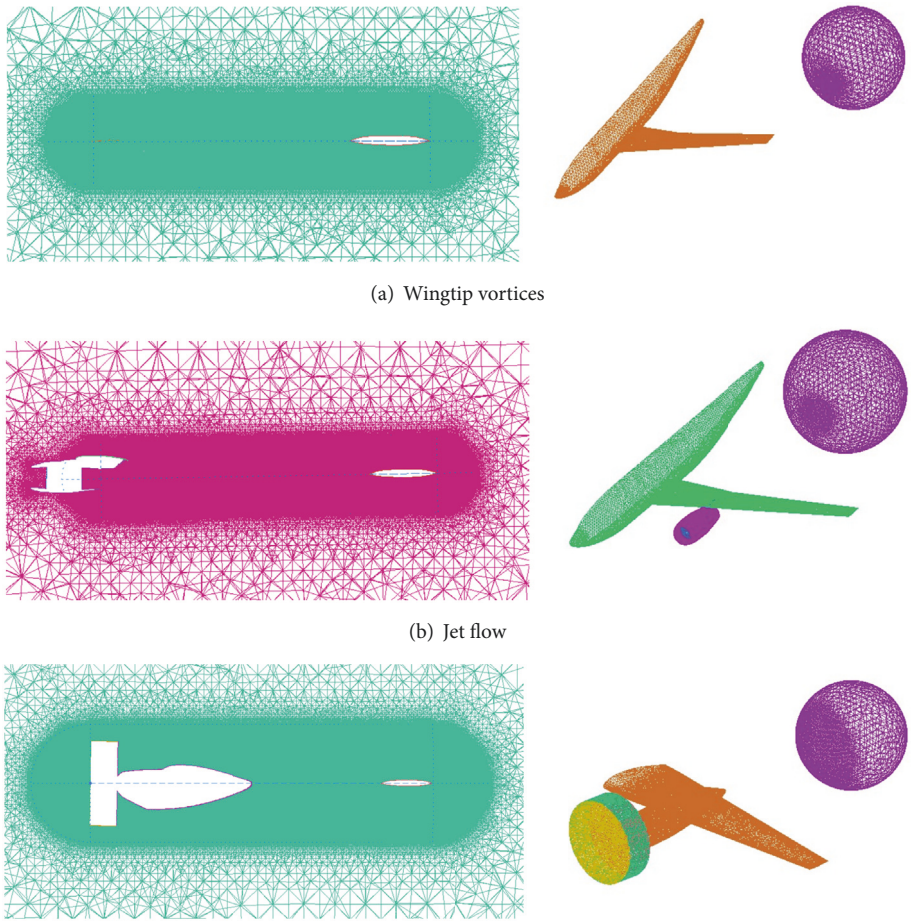

(a) Wingtip vortices

(b) Jet flow

(c) Propeller slipstream

Figure 6: Computational grids.

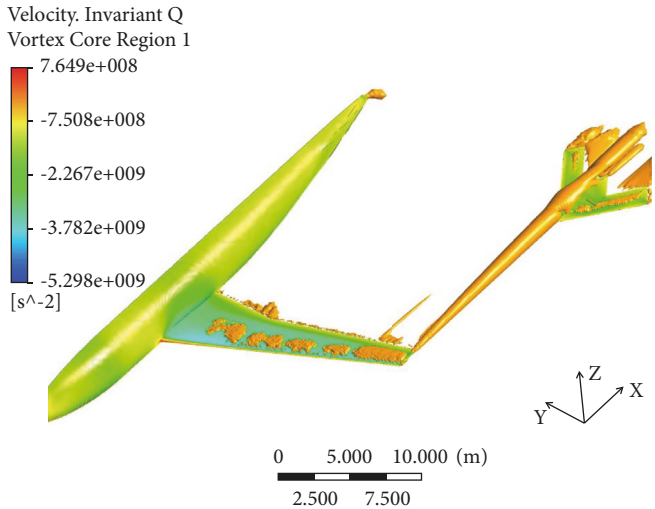

Figure 7: Wingtip vortex extends to the location of fly wing.

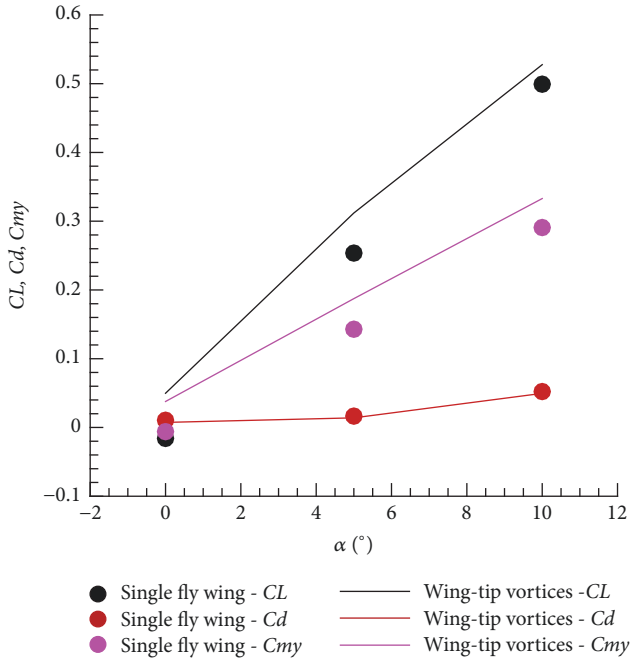

FIGURE 8: Steady aerodynamics-lift coefficients *Cl*, drag coefficients *Cd*, and pitching moment coefficients *Cmy*.

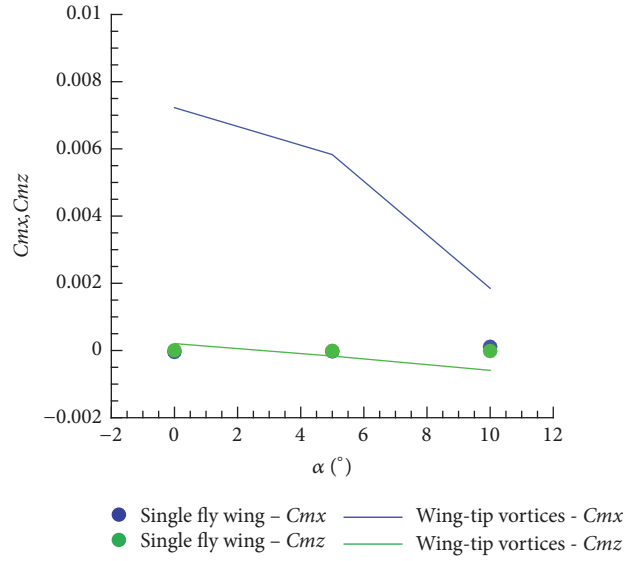

FIGURE 9: Steady aerodynamics, rolling moment coefficients *Cmx* and yawing moment coefficients *Cmz*.

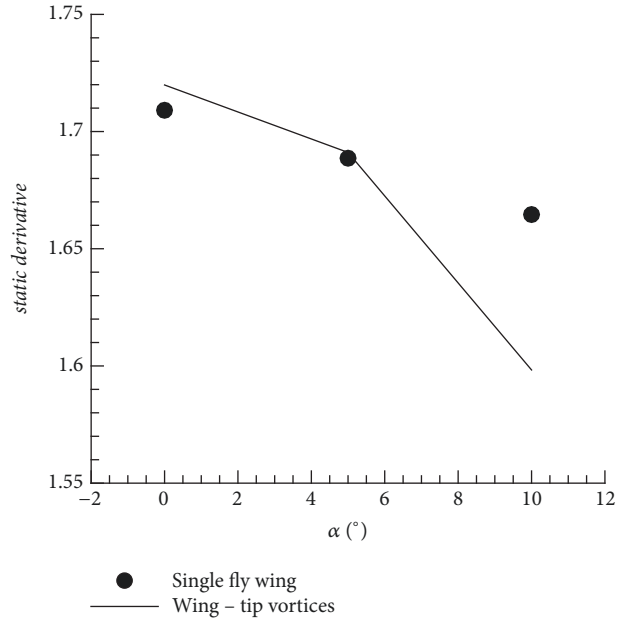

FIGURE 10: Static derivatives $C_{z\alpha}$.

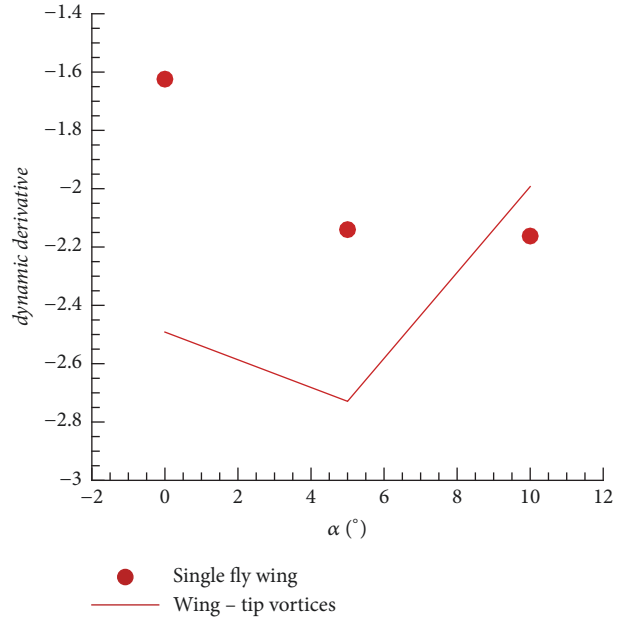

FIGURE 11: Dynamic derivatives $C_{m\dot{\alpha}} + C_{mq}$.

only the aerodynamic and structure characteristics of the flap (mainly refer to the wing flap close to the jet nozzle) but also the flight vehicle behind the flow. We adopt the numerical method and include the inlet and outlet boundary conditions instead of the real engine model to simulate the influence of engine power because this method has been shown to accurately solve this problem. The simulation conditions are the same as those of the wingtip vortices. We still choose the representative cruise mode with a Mach number of 0.7 and altitude of 11 *km*. The attitude of the airliner remains unchanged while the fly wing oscillates around its center of gravity at AoAs of 0°, 5°, and 10°. Unsteady motion can be expressed as $\Delta\alpha = 1^{\circ}\sin(8.6269311t)$ with a corresponding reduced frequency of $k = 0.05$.

Figure 12 displays the flow flied of the airliner with power-on engine, the high temperature and speed jet flow can still downward to the fly wing even it is 20*m* away behind the nozzle, therefore, the local flow flied around the fly wing is changed. The steady aerodynamic coefficients of forces and moments are presented in Figures 13 and 14. Compared with the shear effect of wingtip vortices, the jet flow changes the

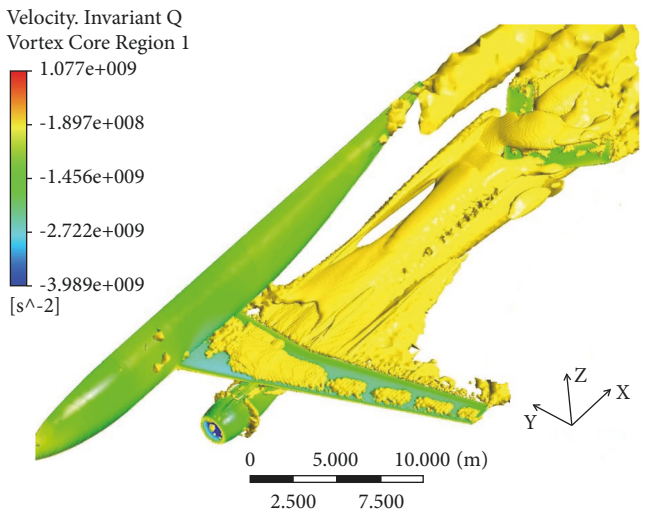

FIGURE 12: Influence of the jet flow on the fly wing.

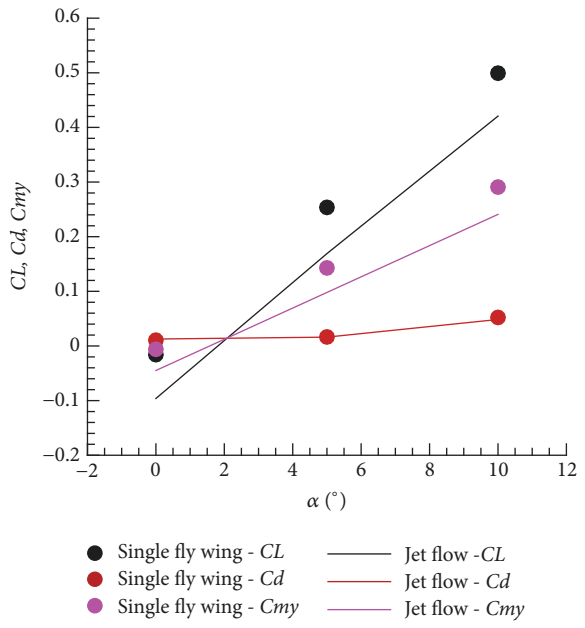

FIGURE 13: Steady aerodynamics-lift coefficients *Cl*, drag coefficients *Cd*, and pitching moment coefficients *Cmy*.

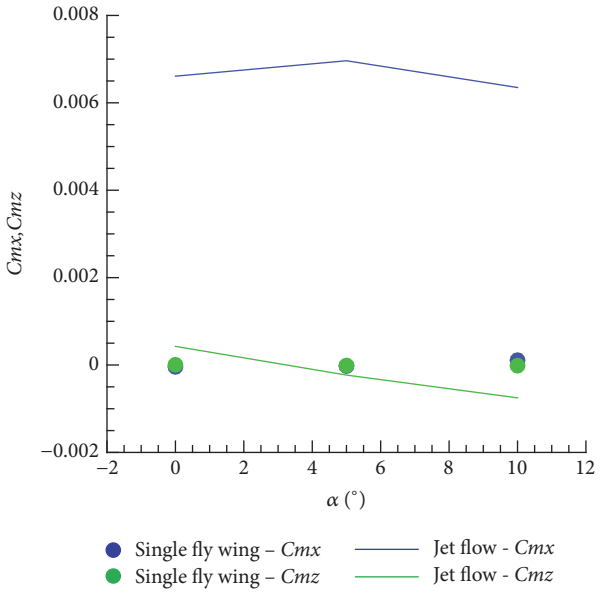

FIGURE 14: Steady aerodynamics, rolling moment coefficients *Cmx* and yawing moment coefficients *Cmz*.

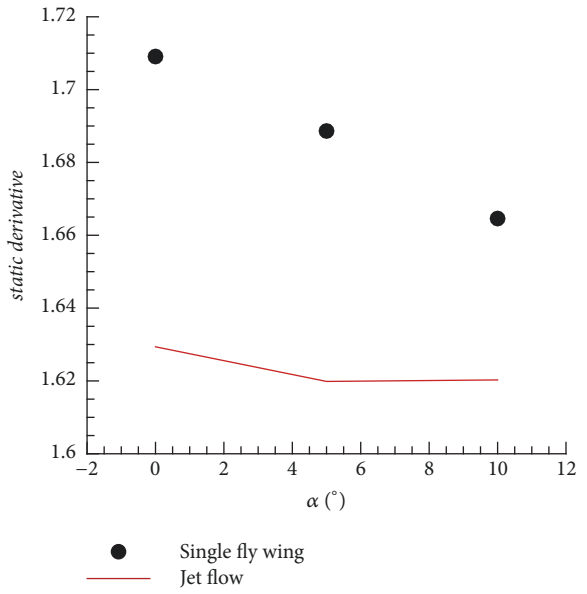

FIGURE 15: Static derivatives $C_{z\alpha}$.

local velocity and direction of the flow around the fly wing, which leads to a decrease in drag and a greater decrease in lift. Thus, the lift-to-drag ratios are reduced at all AoAs. Similar to the effect of wingtip vortices, the pitching and yawing characteristics do not show considerable differences compared with normal cases, whereas the asymmetric aerodynamics on two sides of the fly wing cause a huge change in the rolling moment. However, note that the change in the rolling moment is closely related to the position of the fly wing behind the engine.

Figures 15 and 16 show the static and dynamic derivatives of the fly wing, respectively. Compared with normal flight, the jet flow has an obvious effect on the static and dynamic characteristics. The static stability remains weakly unstable because of the smaller positive values of derivatives, and the absolute values of the dynamic derivatives with increments of the AoA are less than those of the single fly wing cases, indicating that the dynamic damping is diminished with the jet flow. All the changes of the static and dynamic characteristics should be determined in detail, and the attitude of the fly wing should be adjusted in real time.

4.3. Effect of Propeller Slipstream. The propeller of a plane has its own characteristics, and the simulation conditions are different from those of the previous calculations. The

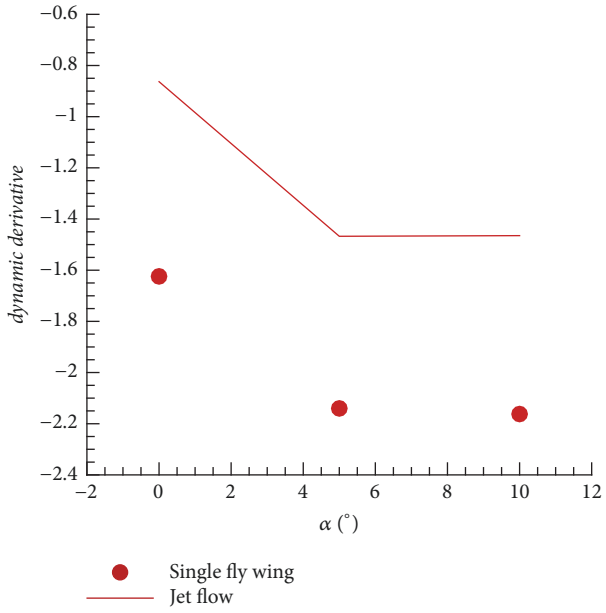

Figure 16: Dynamic derivatives $C_{m\dot{\alpha}} + C_{mq}$.

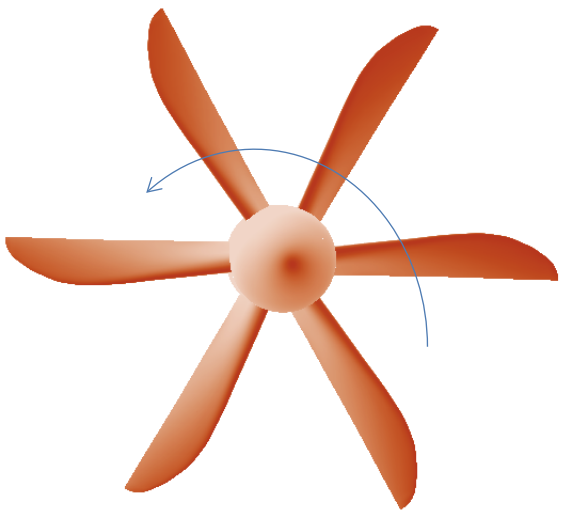

Figure 17: The counterclockwise rotation of the propeller.

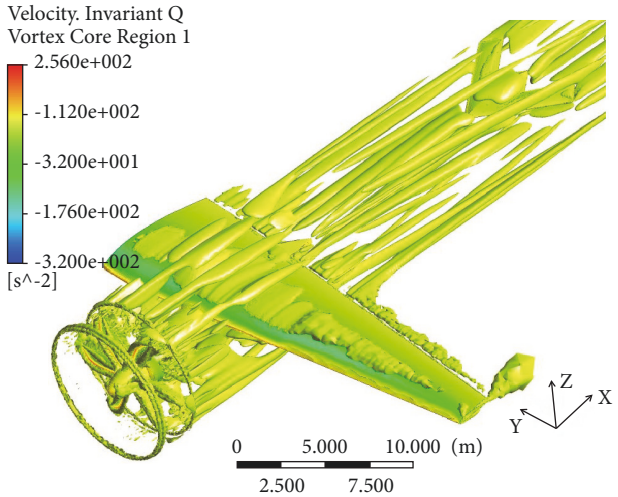

Figure 18: Propeller slipstream effect on the fly wing.

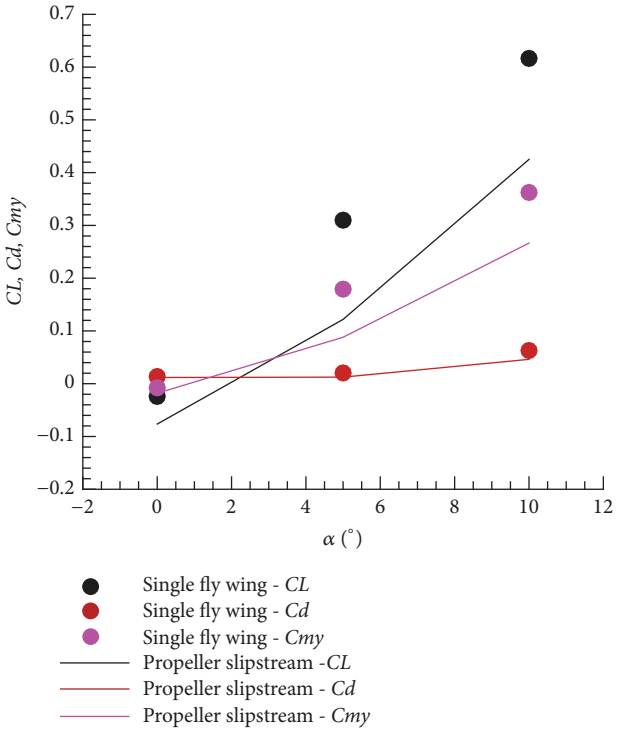

Figure 19: Steady aerodynamics-lift coefficients *Cl*, drag coefficients *Cd*, and pitching moment coefficients *Cmy*.

Mach number of the freestream is assumed to be Ma=0.55, the cruising altitude is 8 km, and the unsteady motion is described as $\Delta\alpha = 1^{\circ}\sin(7.075595t)$ at the three AoAs considered. The counterclockwise rotation speed of the propeller with 6 blades is n_s=1080 rev/min (Figure 17), and the sliding mesh is used to simulate the unsteady motion of the propeller.

The propeller slipstream is much more serious than the wingtip vortices and the jet flow because the long range of the flow region with high speed air rotation behind the propeller substantially affects the aerodynamics of wingman flight. Figure 18 describes the vorticity of the propeller slipstream. As the interruption of the wing and the engine nacelle, the slipstream is weakened but still moves to downstream and affects the aerodynamics of the fly wing. Figures 19 and 20 present the steady forces and moments of the fly wing. The corresponding results indicate that the lift and drag as well as the lift-to-drag ratio decrease at these AoAs, whereas the pitching and yawing moments have no significant difference relative to those of normal flight. Furthermore, the rolling moment suffers heavy interference from the synthesis speed of the rotating flow.

The static and dynamic derivatives are shown in Figures 21 and 22. The static derivatives at these three AoAs remain positive and the values become larger than those of the case

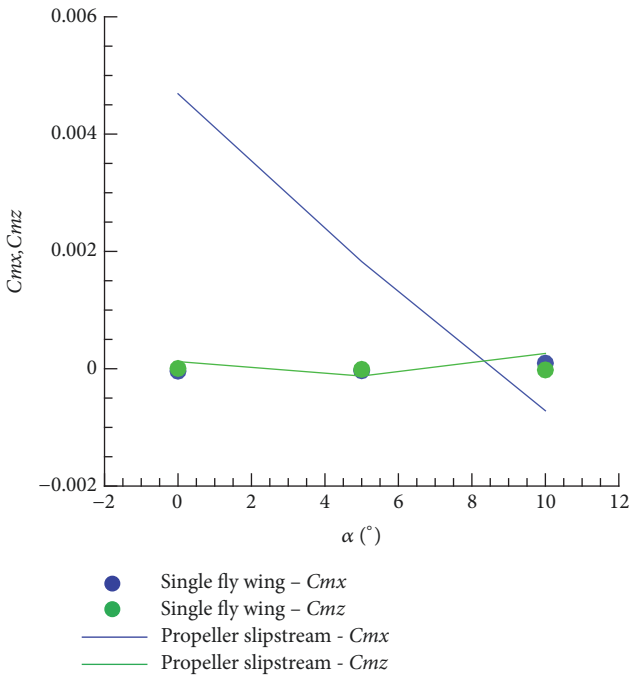

Figure 20: Steady aerodynamics, rolling moment coefficients *Cmx* and yawing moment coefficients *Cmz*.

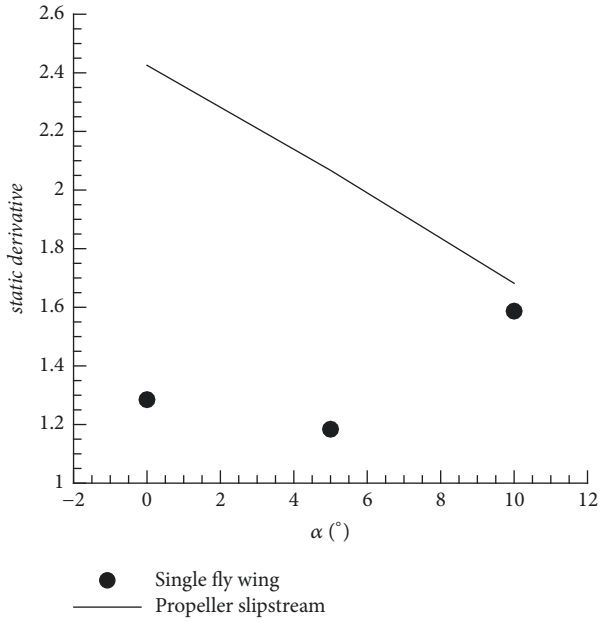

Figure 21: Static derivatives $C_{z\alpha}$.

of no wake flow. However, the trend of the static stability appears to be fairly different. The dynamic characteristics are much more complex, although the trend is the same as that observed for the normal cases. Because of the effect of propeller slipstream, the values of the dynamic derivatives are negative, indicating that the unsteady motions are always accompanied by dynamic damping. The absolute values decrease as the AoA increases because the flow begins to

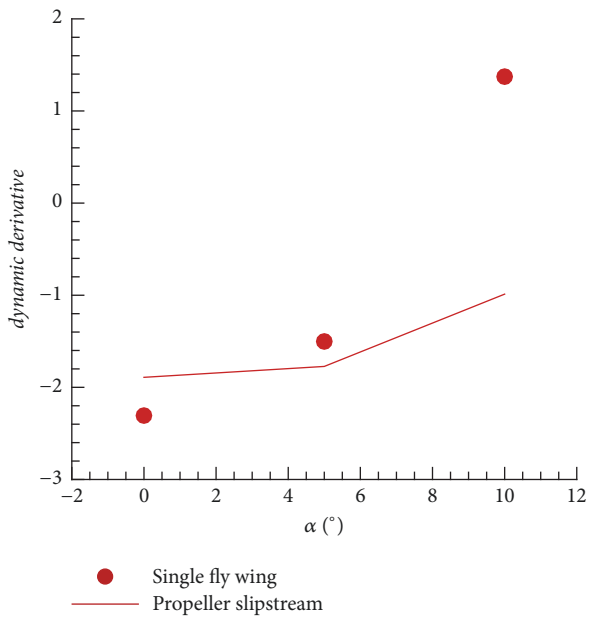

Figure 22: Dynamic derivatives $C_{m\dot{\alpha}} + C_{mq}$.

separate from the leading edge of the fly wing at high AoAs and the dynamic aerodynamics before and after the aerodynamic center are substantially changed. Compared with a single fly wing, the propeller inhibits the change in dynamic stability.

5. Conclusions

In this paper, a novel CFD method based on a sliding mesh technique was proposed to calculate the static and dynamic aerodynamics of three wake flow patterns, and the static and dynamic stability derivatives were identified by using the least squares method. The conclusions can be summarized as follows:

(1) The least squares method can accurately obtain the static and dynamic derivatives.

(2) Wingtip vortices have a strong effect on the fly wing behind the airliner, which enhances the lift-to-drag ratio and rolling moment. The static stabilities in the presence of wingtip vortices have no apparent difference compared with those of the normal flight, whereas the dynamic damping is heavily affected by the wingtip vortices.

(3) The jet flow changes the local velocity and direction of the flow around the fly wing; thus, the lift-to-drag ratio is reduced at all the evaluated AoAs, and the rolling moments are caused by the asymmetric aerodynamics on two sides of the fly wing. The static damping and dynamic damping are both weakened under the effect of jet flow.

(4) The propeller slipstream has a long-range effect behind the aircraft and seriously interferes with the

aerodynamics of the fly wing, which causes the lift-to-drag ratios as well as the lift and drag to decrease at the given AoAs. Moreover, the trend in static stability is different from that of normal flight, although the positive values of the static derivatives become larger, and the propeller slipstream inhibits the change in dynamic stability.

In conclusion, although the static and dynamic aerodynamics of the fly wing under the wake flow patterns were calculated and the derivatives identified, real cases are much more complex. Therefore, high-fidelity CFD methods must be further developed to capture the detailed characteristics of the wake flow, and additional research must be conducted on the influencing factors between aircrafts, such as the distance, position, and altitude.

Data Availability

The data used to support the findings of this study are available from the corresponding author upon request.

Conflicts of Interest

The authors declare that we have no financial and personal relationships with other people or organizations that can inappropriately influence our work; there is no professional or other personal interest of any nature or kind in any products, service, and/or company that could be construed as influencing the position presented in, or the review of, the manuscript entitled.

Acknowledgments

The authors would like to acknowledge the support of National Natural Science Foundation of China (Grant no. 11672236) and Project funded by China Postdoctoral Science Foundation (Grant no. 2018M641381). Part of the previous work was finished by Mrs. Lu Sisi; we also gratefully acknowledge her contribution.

References

[1] C. Hwang and W. Pit, "Aircraft wake flow effect and horizontal tail buffet," *Journal of Aircraft*, vol. 16, no. 4, pp. 282–284, 1979.

[2] I. G. Sheldon, *Wing Tip Vortices*, Springer Publishing, Germany, 1995.

[3] D. P. Rizzetta, M. R. Visbal, and M. J. Stanek, "Numerical investigation of synthetic-jet flowfields," *AIAA Journal*, vol. 37, no. 8, pp. 919–927, 1999.

[4] E. W. M. Roosenboom, A. Stürmer, and A. Schröder, "Advanced experimental and numerical validation and analysis of propeller slipstream flows," *Journal of Aircraft*, vol. 47, no. 1, pp. 284–291, 2010.

[5] J. Dacles-Mariani, S. Rogers, and D. Kwak, "A computational study of wingtip vortex flowfield," in *Proceedings of the 24th Fluid Dynamics Conference, AIAA93-3010*, Orlando, Fla, USA, 1993.

[6] L. Jiang, J. Cai, and C. Liu, "Large-eddy simulation of wing tip vortex in the near field," *International Journal of Computational Fluid Dynamics*, vol. 22, no. 5, pp. 289–330, 2008.

[7] M. J. Churchfield and G. A. Blaisdell, "Numerical simulations of a wingtip vortex in the near field," *Journal of Aircraft*, vol. 46, no. 1, pp. 231–243, 2009.

[8] A. Inasawa, F. Mori, and M. Asai, "Detailed observations of interactions of wingtip vortices in close-formation flight," *Journal of Aircraft*, vol. 49, no. 1, pp. 205–213, 2012.

[9] S. Kasper, T. Burke, J. Rapski, and N. Saneholtz, "Aerodynamics of formation flight for UAVs," in *Proceedings of the AIAA Atmospheric Flight Mechanics Conference, AIAA 2016-1285*, San Diego, Calif, USA, January 2016.

[10] R. Rudnik, C. Rossow, and H. F. V. Geyr, "Numerical simulation of engine/airframe integration for high-bypass engines," *Aerospace Science and Technology*, vol. 6, no. 1, pp. 31–42, 2002.

[11] S. Ritter, "Impact of different UHBR-engine positions on the aerodynamics of a high-liftwing," *Notes on Numerical Fluid Mechanics and Multidisciplinary Design*, vol. 131, pp. 367–380, 2016.

[12] S. Melber-Wilkending, R. Wilhelm, and H. Geyr, "RANS soluations for a complex high-lift configuration of a transport aircraft with engine including improved resolution of the nearfield," in *Proceedings of the 22nd Applied Aerodynamics Conference and Exhibit, AIAA 2004-5081*, Providence, RI, USA, 2004.

[13] M. J. T. Schroijen and R. Slingerland, "Propeller slipstream effects on directional aircraft control with one engine inoperative," in *Proceedings of the 45th AIAA Aerospace Sciences Meeting and Exhibit, AIAA 2007-1046*, pp. 12592–12604, Reno, Nev, USA, January 2007.

[14] F. Moens and P. Gardarein, "Numerical simulation of the propeller/wing interactions for transport aircraft," in *Proceedings of the 19th AIAA Applied Aerodynamics Conference, AIAA 2001-2404*, Anaheim, Calif, USA, June 2001.

[15] C. Lenfers, N. Beck, and M. Bauer, "Propeller and active high lift wing interaction in experiment and simulation," in *New Results in Numerical and Experiment Fluid Mechanics X*, Springer International Publishing, 2014.

[16] H. Xu, Z. Ye, and A. Shi, "Numerical study of propeller slipstream based on unstructured dynamic overset grids," *Journal of Aircraft*, vol. 49, no. 2, pp. 384–389, 2012.

[17] W. Khan, R. Caverly, and M. Nahon, "Propeller slipstream model for small unmanned aerial vehicles," in *Proceedings of the AIAA Modeling and Simulation Technologies (MST) Conference, AIAA 2013-4907*, Boston, Mass, USA, August 2013.

[18] R. Paul and W. L. Garrard, "Dynamic and control of tailless aircraft," in *Proceedings of the 22nd Atmospheric Flight Mechanics Conference, AIAA1997-3776*, August 1997.

[19] S. Esteban, "Static and dynamic analysis of an unconventional plane: flying wing," in *Proceedings of the AIAA Atmospheric Flight Mechanics Conference and Exhibit, AIAA Paper 2001-4010*, Montreal, Canada, August 2001.

[20] F. R. Menter, "Two-equation eddy-viscosity turbulence models for engineering applications," *AIAA Journal*, vol. 32, no. 8, pp. 1598–1605, 1994.

[21] S. H. Park, Y. Kim, and J. H. Kwon, "Prediction of dynamic damping coefficients using unsteady dual-time stepping method," in *Proceedings of the 40th AIAA Aerospace Sciences Meeting and Exhibit, AIAA 2002-0715*, Reno, Nev, USA, January 2002.

[22] L. L. Green, Spence A. M., and P. C. Murphy, "Computation methods for dynamic stability and control derivatives," in *Proceedings of the AIAA Atmospheric Flight Mechanics Conference, AIAA 2004-0015*, Reno, Nevada, USA, 2004.

[23] D. V. Dan, D. L. Thomas, and S. Andreas, "SACCON forced oscillation tests at DNW-NWB and NASA Langley 14×22-foot tunnel," in *Proceedings of the 28th AIAA Applied Aerodynamics Conference, AIAA 2010-4394*, Chicago, Ill, USA, July 2010.

[24] J.-F. Le Roy, S. Morgand, and D. Farcy, "Static and dynamic derivatives on generic UCAV without and with leading edge control," in *Proceedings of the 32nd AIAA Applied Aerodynamics Conference, AIAA 2014-2391*, Atlanta, Ga, USA, June 2014.